

Thermalization of a color glass condensate and review of the “Bottom-Up” scenario

Andrej El¹ *, Zhe Xu^{1†} and Carsten Greiner^{1 ‡}

¹*Institut für Theoretische Physik, Johann Wolfgang Goethe-Universität Frankfurt,
Max-von-Laue-Str.1, D-60438 Frankfurt am Main, Germany*

(Dated: August 28, 2021)

Abstract

The thermalization of a longitudinally expanding color glass condensate with Bjorken boost invariant geometry is investigated within microscopical parton cascade BAMPS. Our main focus lies on the detailed comparison of thermalization, observed in BAMPS with that suggested in the “Bottom-Up” scenario. We demonstrate that the tremendous production of soft gluons via $gg \rightarrow ggg$, which is shown in the “Bottom-Up” picture as the dominant process during the early preequilibration, will not occur in heavy ion collisions at RHIC and LHC energies, because the back reaction $ggg \rightarrow gg$ hinders the absolute particle multiplication. Moreover, contrary to the “Bottom-Up” scenario, soft and hard gluons thermalize at the same time. The time scale of thermal equilibration in BAMPS calculations is of order $\alpha_s^{-2}(\ln \alpha_s)^{-2}Q_s^{-1}$. After this time the gluon system exhibits nearly hydrodynamical behavior. The shear viscosity to entropy density ratio has a weak dependence on Q_s and lies close to the lower bound of the AdS/CFT conjecture.

PACS numbers: 25.75.-q, 12.38.Mh, 05.60.-k, 24.10.Lx

* E-mail: el@th.physik.uni-frankfurt.de

† E-mail: xu@th.physik.uni-frankfurt.de

‡ E-mail: carsten.greiner@th.physik.uni-frankfurt.de

I. INTRODUCTION

The success of employing simple ideal hydrodynamics [1] in describing the large values of the elliptic flow v_2 measured in Au+Au collisions at the Relativistic Heavy Ion Collider (RHIC) [2, 3] indicates that thermal equilibration of the produced quark gluon system occurs on a short time scale and that the equilibrium is maintained until the hadronization. It is of great interest to understand what mechanisms drive the system to equilibrium. While coherent quantum effects like color instabilities [4] may play a role at the very early stage when the system is super dense, perturbative QCD (pQCD) bremsstrahlung processes are essential for momentum isotropization of quark gluon matter [5, 6] when the matter becomes more dilute due to the strong longitudinal expansion.

The importance of pQCD bremsstrahlung was first raised in the “Bottom-Up” scenario [7], which describes the thermal equilibration of a color glass condensate [8, 9] characterized by a saturation scale Q_s . The main idea of the “Bottom-Up” scenario is that while the hard gluons with transverse momenta of order Q_s degrade as the condensate evolves in space time, soft gluons with transverse momenta much smaller than Q_s are populated due to pQCD $gg \rightarrow ggg$ bremsstrahlung. Soft gluon production dominates the early stage of equilibration and a strong parametric enhancement of the soft gluon number has been predicted. Within a short time scale the soft gluon number becomes comparable to the initial number of hard gluons. As soon as the radiated soft gluons achieve thermal equilibrium and build up a thermal bath, the hard ones begin to lose their energy to the thermal bath and subsequently thermalize on a later time scale. A parametric time scale for overall thermalization is given by $\tau_{\text{th}} \sim \alpha_s^{-13/5} Q_s^{-1}$ [7].

Because color glass condensate (CGC) [8] is proposed as a possible initial state of the quark gluon matter produced in high energy heavy ion collisions, its thermalization is a highly interesting topic. For instance, the thermalization of an idealized form of color glass condensate [10] was studied by Bjorker and Venugopalan by [11] solving the Landau transport equation. Serreau and Schiff also investigated the same topic in [12] where they used the relaxation time approximation to simplify the collision term in the Boltzmann equation. A conclusion, which can be drawn from the two studies, is that pQCD $gg \rightarrow gg$ collisions are not sufficient to achieve thermal equilibrium. Hence, the inelastic $gg \leftrightarrow ggg$ processes are needed as emphasized in the “Bottom-Up” scenario.

The role of the pQCD $gg \leftrightarrow ggg$ processes for thermal equilibration employing the color glass condensate initial condition is investigated in the present work for the first time within a full 3+1 dimensional transport calculation using the parton cascade BAMPS [13]. The bremsstrahlung processes indeed lead to rapid thermalization. In this paper we focus on how thermalization occurs in BAMPS calculations. In particular, we investigate whether the “Bottom-Up” scenario is realized as the proper way to describe thermalization of CGC, which may be formed in heavy ion collisions at RHIC and LHC energies. Note that the back reactions of the bremsstrahlung, i.e., $ggg \rightarrow gg$ processes, are consistently incorporated in BAMPS, whereas they are missing in the “Bottom-Up” scenario. This, which is shown in our results, leads to a different thermalization picture from the one suggested by the “Bottom-Up” scenario.

This paper is organized as follows. In section II we present the parton cascade BAMPS and the setup. A boundary condition is introduced to mimic a one-dimensional (longitudinal) expansion with Bjorken boost invariance. In section III the detail on the CGC initial conditions is given. The importance of $ggg \rightarrow gg$ processes, which hinders the multiplication of soft gluons, is discussed in section IV. The numerical results based on BAMPS calculations are shown in section V. We compare the thermalization observed in BAMPS with the “Bottom-Up” scenario, determine the time scale of thermal equilibration for various saturation scales Q_s and coupling constants α_s and extract the shear viscosity to entropy density ratio, η/s . A conclusion is given in section VI.

II. PARTON CASCADE BAMPS

BAMPS is a microscopical transport model, which solves the Boltzmann equations for on-shell quarks and gluons using Monte Carlo techniques. In the present work only gluons are considered. The main feature of BAMPS is the implementation of $2 \rightarrow N$ and $N \rightarrow 2$ processes in a consistent manner, which is based on the stochastic interpretation of interaction rates [5]. The interaction rates or the interaction probabilities are calculated locally in space where the phase space density of particles, $f(p, x)$, is extracted numerically. BAMPS subdivides space into small cells, which are regarded as the local positions where interactions may occur. The smaller the cells the more local interactions can be realized. However, smaller cells contain fewer particles and thus lead to larger uncertainties in the extraction

of $f(p, x)$. Therefore, we adopt the test particle method to amplify the (pseudo)particle density by a factor N_{test} . The cross sections have to be reduced by the same factor to obtain the same physical mean free path [5].

In order to make comparisons with the ‘‘Bottom-Up’’ scenario we calculate the space time evolution of gluons in a tube with a radius of $R = 5$ fm. The transverse wall of the tube serves as a boundary to mimic one-dimensional (longitudinal) expansion. Gluons are simply reflected on the cylindrical wall. In the transverse plan a static ‘‘spider web’’ like cell structure is considered: The polar angle ϕ and the radial length squared r^2 are divided equally within $[0, 2\pi]$ and $[0, R^2]$, respectively. This division gives the same transverse area for all cells. For the numerical calculations we set $\Delta\phi = \pi/4$ and $\Delta r^2 = 5 \text{ fm}^2$. Longitudinally, space is divided in Δz bins, which have the same width in the space time rapidity $\eta = \frac{1}{2} \ln((t+z)/(t-z))$. $\Delta\eta = 0.2$ is set to be a constant for all Δz bins. The initial gluons are put into rapidity interval $[-3; 3]$. Our setup is adequate to the assumption of Bjorken boost invariance [14], which is used in this study.

Gluon interactions included in BAMPS are elastic pQCD $gg \rightarrow gg$ scatterings as well as pQCD inspired bremsstrahlung $gg \leftrightarrow ggg$. The differential cross sections and the effective matrix elements are given by [15, 16, 17]

$$\frac{d\sigma^{gg \rightarrow gg}}{dq_{\perp}^2} = \frac{9\pi\alpha_s^2}{(q_{\perp}^2 + m_D^2)^2}, \quad (1)$$

$$|\mathcal{M}_{gg \rightarrow ggg}|^2 = \frac{9g^4}{2} \frac{s^2}{(\mathbf{q}_{\perp}^2 + m_D^2)^2} \frac{12g^2 \mathbf{q}_{\perp}^2}{\mathbf{k}_{\perp}^2 [(\mathbf{k}_{\perp} - \mathbf{q}_{\perp})^2 + m_D^2]} \Theta(k_{\perp} \Lambda_g - \cosh y) \quad (2)$$

where $g^2 = 4\pi\alpha_s$. \mathbf{q}_{\perp} and \mathbf{k}_{\perp} denote the perpendicular component of the momentum transfer and of the radiated gluon momentum in the center-of-mass frame of the collision, respectively. y is the momentum rapidity of the radiated gluon in the center-of-mass frame, and Λ_g is the gluon mean free path, which is calculated self consistently [5]. A discussion of the present idealistic implementation of the LPM effect is given in [6].

The interactions of the massless gluons are screened by a Debye mass

$$m_D^2 = \pi d_G \alpha_s \int \frac{d^3p}{(2\pi)^3 p} N_c f_g \quad (3)$$

where $d_G = 16$ is the gluon degeneracy factor for $N_c = 3$. m_D is calculated locally using the gluon density function $f(p, x)$ obtained from BAMPS. The suppression of bremsstrahlung due to the Landau-Pomeranchuk-Migdal effect is taken into account within the Bethe-Heitler regime using a step function in Eq. (2).

The interaction rates per particle are obtained [5] by

$$R_{22} = n \langle v_{\text{rel}} \sigma_{22} \rangle_2, \quad (4)$$

$$R_{23} = n \langle v_{\text{rel}} \sigma_{23} \rangle_2, \quad (5)$$

$$R_{32} = \frac{1}{2} n^2 \left\langle \frac{I_{32}}{8E_1 E_2 E_3} \right\rangle_3 \quad (6)$$

for $gg \rightarrow gg$, $gg \rightarrow ggg$, and $ggg \rightarrow gg$, respectively, where

$$\sigma_{22} = \frac{1}{2!} \int_0^{s/4} dq_{\perp}^2 \frac{d\sigma^{gg \rightarrow gg}}{dq_{\perp}^2}, \quad (7)$$

$$\sigma_{23} = \frac{1}{2s} \frac{1}{3!} \int d\Gamma'_1 d\Gamma'_2 d\Gamma'_3 |\mathcal{M}_{gg \rightarrow ggg}|^2 (2\pi)^4 \delta^{(4)}(p_1 + p_2 - p'_1 - p'_2 - p'_3), \quad (8)$$

$$I_{32} = \frac{1}{2!} \int d\Gamma'_1 d\Gamma'_2 |\mathcal{M}_{ggg \rightarrow gg}|^2 (2\pi)^4 \delta^{(4)}(p_1 + p_2 + p_3 - p'_1 - p'_2) \quad (9)$$

where $d\Gamma'_i = d^3 p'_i / (2\pi)^3 2E'_i$, $|M_{ggg \rightarrow gg}|^2 = |M_{gg \rightarrow ggg}|^2 / d_G$, s is the invariant mass for the interaction, $v_{\text{rel}} = s/2E_1 E_2$ denotes the relative velocity of two incoming gluons and $\langle \cdot \rangle_2$ and $\langle \cdot \rangle_3$ symbolize the average within ensembles of incoming gluon pairs and triplets, respectively. For each gluon pair and triplet positioned in a cell unit with volume ΔV the transition probability within a time interval Δt is given [5] by

$$P_{22} = v_{\text{rel}} \sigma_{22} \frac{\Delta t}{\Delta V}, \quad (10)$$

$$P_{23} = v_{\text{rel}} \sigma_{23} \frac{\Delta t}{\Delta V}, \quad (11)$$

$$P_{32} = \frac{I_{32}}{8E_1 E_2 E_3} \frac{\Delta t}{\Delta V^2}, \quad (12)$$

respectively, as derived directly from the transition rates (4)-(6). Note that $R_{32} = 3R_{23}/2$ for thermal equilibrium. The factor $3/2$ indicates the ratio of the number of identical particles in the initial state of the $ggg \rightarrow gg$ and $gg \rightarrow ggg$ interaction.

III. CGC INITIAL CONDITIONS

For the initial condition a gluon distribution of a color glass condensate [8] is applied. The theory of a color glass condensate is given by the saturation picture, which assumes that the parton distribution in a hadron or nuclei saturates at high energies as a result of competition between QCD bremsstrahlung and annihilation processes.

The CGC initial condition used in our simulations consists of gluons with $p_T < Q_s$, which are produced by the nonperturbative part of the nucleus-nucleus interaction. Q_s denotes

the saturation momentum, which is the typical momentum of gluons in the CGC. It is close to 2 GeV at RHIC and is expected to be $4 - 6 \text{ GeV}$ at LHC[18]. The color glass condensate is a state with high parton occupation number where the transverse momenta reach up to Q_s , whereas the occupation number drops to 0 for transverse momenta much larger than Q_s . Initially, most gluons have transverse momenta close to Q_s , whereas the longitudinal momentum of gluons in the central rapidity bin is approximately zero.

For the initial gluon distribution of Color Glass Condensate we employ an idealized and boost-invariant form [11]

$$f(x, p) = \frac{c}{\alpha_s N_c} \frac{1}{\tau} \delta(y - \eta) \Theta(Q_s^2 - p_T^2) \quad (13)$$

We take $N_c = 3$ for SU(3). The factor c in (13) is the ‘‘parton liberation coefficient’’ which accounts for the transformation of virtual partons in the initial state into on-shell partons in the final state, as introduced in [20]. The value of c used in [11] was calculated for a SU(2) gauge theory to be $c = 1.3$ [9]¹. New SU(3) gauge theory calculations yield a value of $c \simeq 0.4$ [18, 19], which we employ for the following calculations.

The initial particle density in the CGC approach is given by [10, 11]

$$\frac{1}{\pi R^2} \frac{dN}{d\eta} = c \frac{N_c^2 - 1}{4\pi^2 \alpha_s N_c} Q_s^2 \quad (14)$$

For the application of the Boltzmann equation, we need the phase space density to be smaller than unity. If phase space density is high, Bose enhancement factors should be considered in the collision integrals, which is not done in BAMPS model.

The initial gluons are produced at eigentime $\tau \sim \frac{1}{Q_s}$ and the initial phase space density $f(x, p)$ from Eq.(13) is infinite due to the delta function $\delta(p_z) \sim \frac{1}{\Delta p_z}$. Later the distribution in longitudinal momentum space broadens due to $2 \rightarrow 2$ (or $2 \rightarrow 3$) collisions and the occupation number becomes finite. Our cascade starts at time $\tau_0 = \frac{c}{\alpha_s N_c} \tau_i$ where $\tau_i \cong \frac{1}{Q_s}$. At this time the parton distribution function in Eq.(13) is still larger than unity. However, the same initial time has been applied in [11]. In the ‘‘Bottom-Up’’ picture at a time $\tau \sim \alpha_s^{-3/2} Q_s^{-1}$ the distribution should become less than 1. We note that we do not employ the Bose enhancement factor $(1 + f)$ within the Boltzmann collision terms. Hence, as long as f is larger than 1 we underestimate the rates.

¹ This value we used in our previous calculations [21, 22].

In the following we present the results of simulations for $Q_s = 2, 3$ and 4 GeV , i.e., energies relevant for RHIC and LHC.

IV. SOFT GLUON PRODUCTION AND ANNIHILATION

The basic assumption of the “Bottom-Up” thermalization picture is that soft gluons are continually emitted due to inelastic $2 \rightarrow 3$ bremsstrahlung processes, which increase in the soft the gluon number and leads to formation of a thermal bath. However, the annihilation processes, which are the back reactions of bremsstrahlung and missing are in the “Bottom-Up” scenario, will hinder the soft gluon production due to detailed balance. The annihilation processes become dominant, when the system is oversaturated. Using the CGC initial conditions in Eq.(14) we estimate whether a net production of gluons is possible during the subsequent space time evolution.

Assuming a free streaming of CGC initial condition, the energy and particle densities are given by

$$e(\tau) = e(\tau_0) \frac{\tau_0}{\tau} = c \frac{N_c^2 - 1}{6\pi^2 \alpha_s N_c} Q_s^3 \frac{1}{\tau}, \quad (15)$$

$$n(\tau) = n(\tau_0) \frac{\tau_0}{\tau} = c \frac{N_c^2 - 1}{4\pi^2 \alpha_s N_c} Q_s^2 \frac{1}{\tau}. \quad (16)$$

Also assuming an instantaneous thermalization at time τ_{th} with

$$e(\tau_{\text{th}}) = e_{\text{th}}(\tau_{\text{th}}) = \frac{48}{\pi^2} T^4(\tau_{\text{th}}), \quad (17)$$

one obtains

$$n_{\text{th}}(\tau_{\text{th}}) = \frac{16}{\pi^2} T^3(\tau_{\text{th}}) = \frac{16}{\pi^2} \left(\frac{1}{288} \frac{N_c^2 - 1}{\alpha_s N_c} c Q_s^3 \right)^{\frac{3}{4}} \left(\frac{1}{\tau_{\text{th}}} \right)^{\frac{3}{4}}. \quad (18)$$

The ratio

$$\frac{n_{\text{th}}(\tau_{\text{th}})}{n(\tau_{\text{th}})} = 24 \left(\frac{1}{108} \right)^{\frac{3}{4}} \alpha_s^{\frac{1}{4}} c^{-\frac{1}{4}} Q_s^{\frac{1}{4}} \tau_{\text{th}}^{\frac{1}{4}} \quad (19)$$

estimates whether a net production or a net reduction of gluons will occur at the early times of the expansion. If the ratio $n_{\text{th}}(\tau_{\text{th}})/n(\tau_{\text{th}})$ is larger than 1, more particles should be produced. Fig. 1 depicts the $n_{\text{th}}(\tau_{\text{th}})/n(\tau_{\text{th}})$ ratio for fixed $Q_s = 3 \text{ GeV}$ and various values of α_s as a function of the thermalization time τ_{th} . All curves start at values smaller than 1, which indicates that for the chosen parameters indeed the annihilation processes would dominate the early stage of equilibration. For an increase of the gluon number at early times,

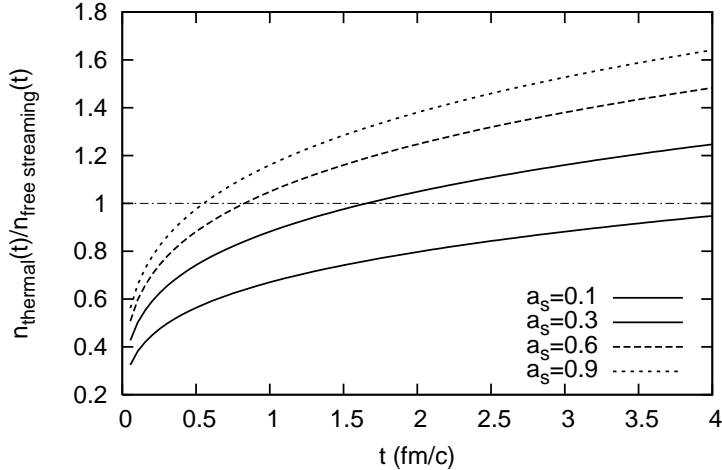


FIG. 1: $n_{\text{th}}(\tau_{\text{th}})/n(\tau_{\text{th}})$ ratio in Eq. (19) as a function of τ_{th} for $Q_s = 3$ GeV and $\alpha_s = 0.1, 0.3, 0.6$, and 0.9 , respectively.

as predicted in the “Bottom-Up” scenario, the value of α_s has to be much larger than 0.3 , or Q_s has to be chosen much larger than would be given at RHIC and LHC. For small coupling the particle number will start growing if the time scale of thermalization is large. In the full calculation of the Boltzmann equation the gluon thermalization is more complicated than the simple consideration of a free streaming and a subsequent instantaneous equilibration. However, the behavior of the $n_{\text{th}}(\tau)/n(\tau)$ ratio holds, as we will shortly see.

The initial distribution of gluons is highly anisotropic in momentum space. Most gluons have a transverse momentum of order $p_t \sim Q_s$. Populations of the low (high) momentum gluons should be dominated by $2 \rightarrow 3$ ($3 \rightarrow 2$) processes. Figure 2 shows the gluon p_t spectra after one single $2 \rightarrow 3$ or $3 \rightarrow 2$ interaction. While $3 \rightarrow 2$ processes increase gluon number in high momenta, $2 \rightarrow 3$ collisions lead to an enhancement of gluon number in soft momenta, which resembles the “Bottom-Up” scenario.

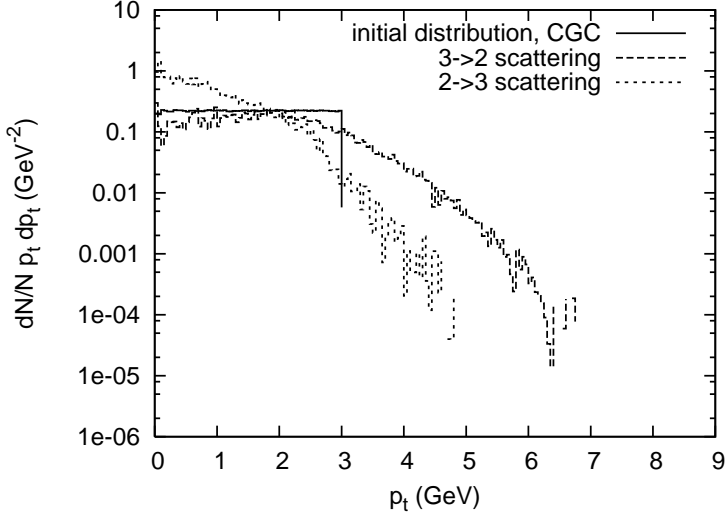


FIG. 2: Transverse momentum distribution after one single inelastic scattering. Initial condition is a CGC with $\alpha_s = 0.3$ and $Q_s = 3$ GeV.

V. RESULTS: THERMALIZATION OF A CGC

A. Gluon number

Fig. 3 shows the gluon multiplicities per space time rapidity, $dN/d\eta$, at midrapidity ($\eta \in [-0.1, 0.1]$) as function of time, which are obtained using BAMPS with the CGC initial conditions with $\alpha_s = 0.3$ and $Q_s = 2, 3,$ and 4 GeV, respectively. Their ratios to the initial gluon number are depicted in Fig. 4. The way that thermalization proceeds within the parton cascade calculations does not resemble the way that has been advocated in the “Bottom-Up” scenario [7]. The strong parametric enhancement of the total gluon number at early times, as predicted by “Bottom-Up” scenario, is not observed in the cascade calculations. Instead, gluon annihilation occurs during the first $0.3 - 0.75$ fm/c for $Q_s = 2 - 4$ GeV. This is clearly due to the $3 \rightarrow 2$ annihilation processes and indicates that the initial CGC is oversaturated for the chosen values of α_s and Q_s . Figure 5 shows the interaction rate of both elastic and inelastic processes in the central space time rapidity bin. The rate of $3 \rightarrow 2$ processes is initially significantly higher than that of $2 \rightarrow 3$ processes, which leads to a decrease in the net gluon number at very early times.

The gluon number begins to increase after $t \sim 0.3 - 0.75$ fm/c (depending on the value of Q_s) when the system is close to kinetic equilibrium and a quasi-hydrodynamical cooling

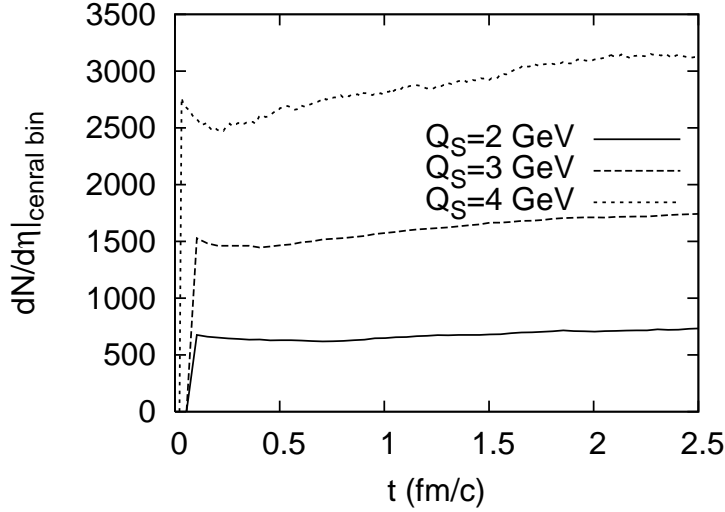


FIG. 3: $dN/d\eta$, at midrapidity ($\eta \in [-0.1, 0.1]$) as a function of time. Results are obtained using BAMPS for the initial CGC with $\alpha_s = 0.3$ and $Q_s = 2, 3,$ and 4 GeV, respectively.

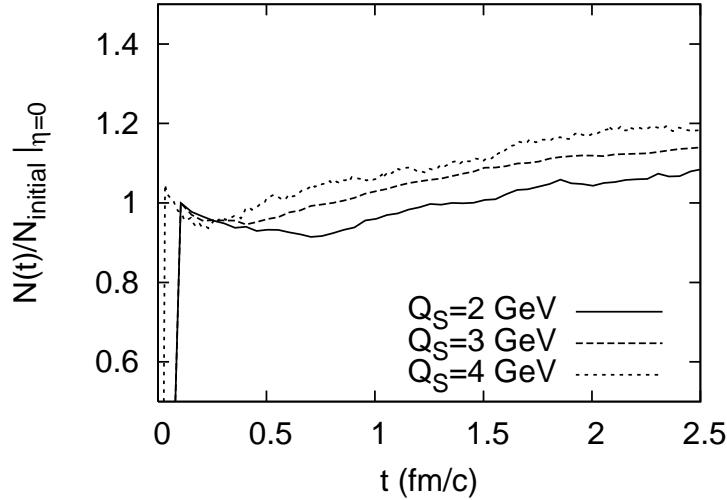


FIG. 4: Ratio of the gluon number to the initial one in the central space time rapidity bin.

sets in. Slow increase in gluon number at late times is consistent with the collision rates, $R_{23} \gtrsim 2R_{32}/3$, shown in Fig. 5. (In chemical equilibrium $R_{23} = 2R_{32}/3$.) Assuming parton-hadron duality, the final gluon multiplicities, $dN/d\eta \approx 700 - 1700$ for $Q_s = 2 - 3$ GeV, are equivalent to $dN_{\text{ch}}/d\eta \approx 470 - 1100$ for the total charged mesons, which are comparable with the RHIC data for Au+Au most central collisions at $\sqrt{s} = 130 - 200$ AGeV [23, 24].

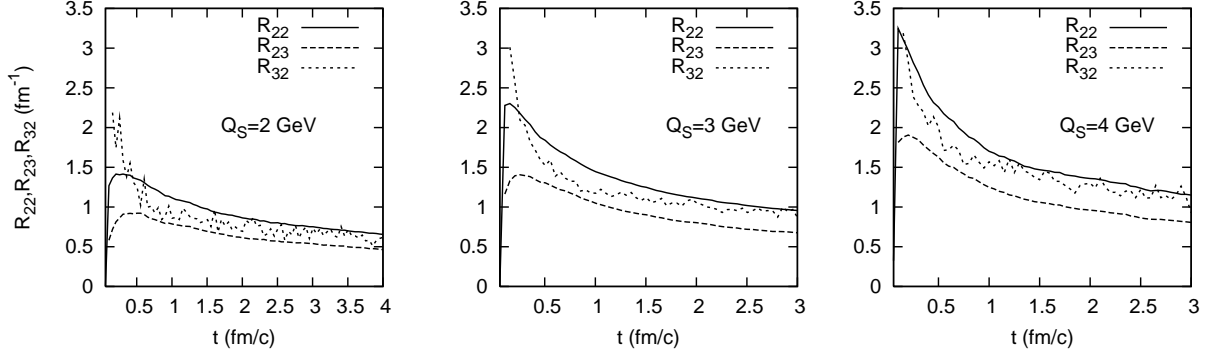


FIG. 5: Interaction rates in the central space time rapidity bin, obtained from BAMPS calculations for CGC with $\alpha_s = 0.3$ and $Q_s = 2, 3,$ and 4 GeV.

As demonstrated in Fig. 2, $2 \rightarrow 3$ collisions lead to an enhancement in the number of the soft gluons, whereas $3 \rightarrow 2$ processes initially increase number of gluons with momenta higher than the saturation momentum Q_s . We now study the changes in gluon momenta for various interaction channels included in the calculations. For this we define a soft momentum scale, which is $p_{\text{soft}}^2 \leq \alpha_s Q_s^2$ in the “Bottom-Up” scenario, to be $p_{\text{soft}} = 1.5$ GeV and a hard scale $p_{\text{hard}} = Q_s$. The medium gluons are denoted as gluons with $p_{\text{soft}} < p_t < p_{\text{hard}}$. These definitions are in particular reasonable at early times since the longitudinal momenta are very small. They are different from the definitions in [7], where the authors set all the initial gluons to be hard. Fig. 6 shows the net gluon production of each type in $2 \rightarrow 3$, $3 \rightarrow 2$, and $2 \rightarrow 2$ processes as function of time. The results are in terms of the difference between the number of outgoing and incoming gluons of each type divided by the number of collisions. We see that $2 \rightarrow 3$ collisions increase the soft gluon number with a loss of medium and hard gluons [see Fig. 6(a)], whereas $3 \rightarrow 2$ processes increase the hard gluon number with the loss of soft and medium gluons [see Fig. 6(b)]. Equivalently, $2 \rightarrow 3$ processes transfer energy from the medium and hard to the soft sector, whereas $3 \rightarrow 2$ processes transfer energy from the soft and medium to the hard sector. Compared to $2 \leftrightarrow 3$ processes, $2 \rightarrow 2$ convert few medium gluons into soft and hard ones [see Fig. 6(c)]. Common to all three collision types in Fig. 6 is a continuous degradation of the medium sector with the simplified CGC initial conditions. As the system evolves towards equilibrium, energy is transferred from the medium into both the soft and hard sector.

The ratio of the numbers of the soft, medium and hard gluons to the total number of

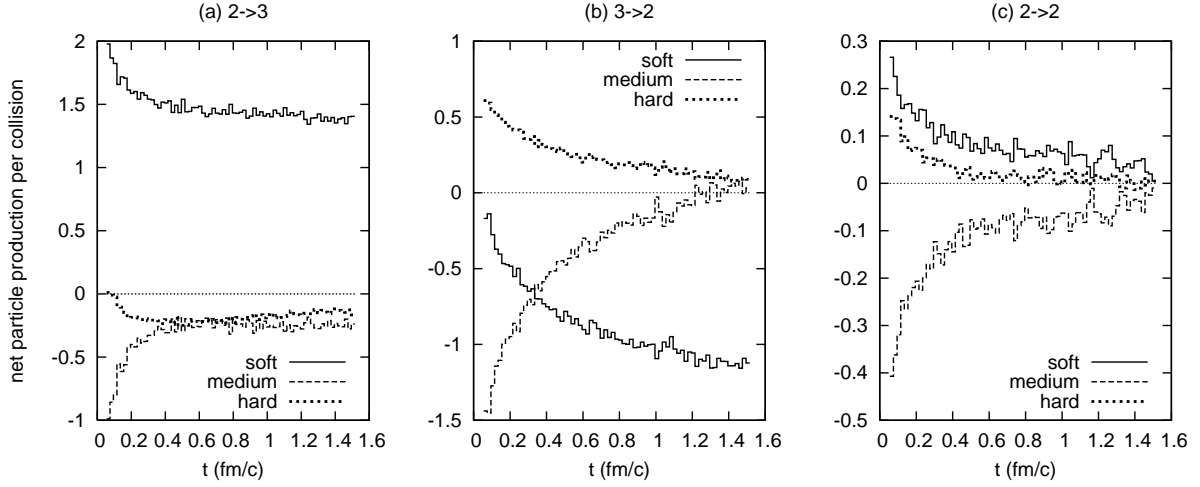


FIG. 6: Net production of soft, medium, and hard gluons in various collisions. Results are obtained in the central space time rapidity bin from a calculation performed for a CGC with $\alpha_s = 0.3$ and $Q_s = 3$ GeV.

gluons is depicted in Fig. 7. The total gluon number is dominated by the medium sector

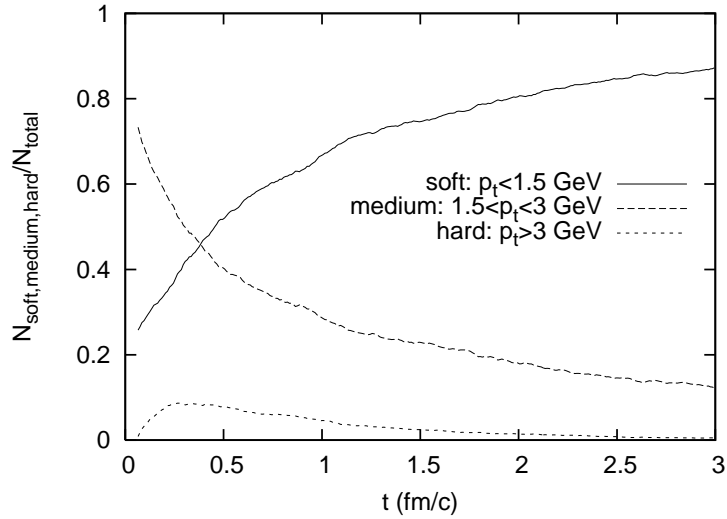


FIG. 7: Ratio of the numbers of the soft, medium and hard gluons to the total number.

until 0.5 fm/c and then by the soft sector after ~ 1 fm/c. Contrary to the “Bottom-Up” picture, Fig. 7 shows that the soft gluon number increases over a long period of time at the cost of the primary “medium” gluons. To repeat, the production of soft gluons is effectively

hindered by $3 \rightarrow 2$ processes and, thus, cannot exhibit a huge increase as predicted in the “Bottom-Up” scenario.

B. Kinetic equilibration and momentum isotropization

Fig. 8 gives the transverse momentum spectra in the central space time rapidity and at various early times (up to 0.5 fm/c) obtained from BAMPS for initial CGC with $\alpha_s = 0.3$ and $Q_s = 3$ GeV. After the expansion starts, energy flows immediately into both the soft

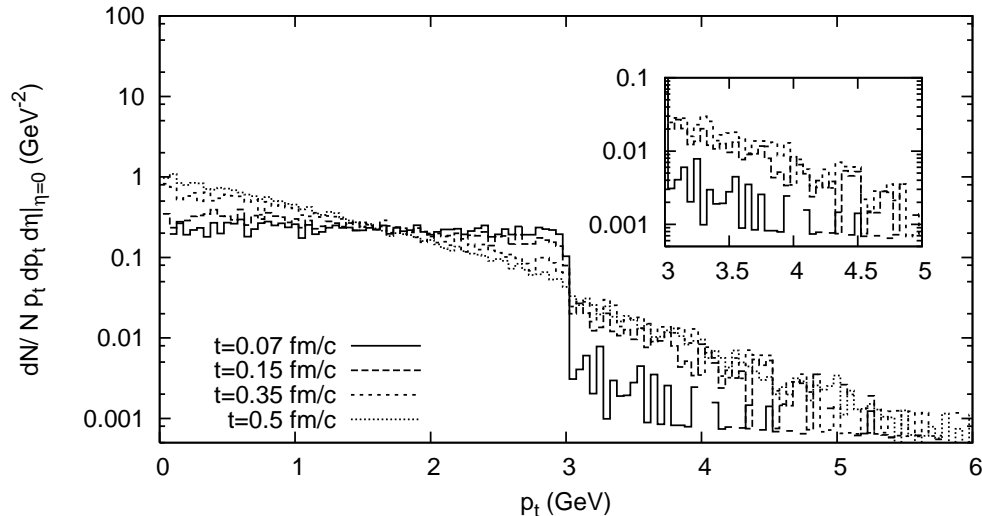


FIG. 8: Transverse momentum spectra in the central space time rapidity and at various early times. The initial condition for the BAMPS calculation is a CGC with $\alpha_s = 0.3$ and $Q_s = 3$ GeV.

($p_t < p_{\text{soft}} = 1.5$ GeV) and hard momentum region ($p_t > Q_s$) where the populations rapidly increase, as also seen in Fig. 7. Note that at 0.5 fm/c the number of soft gluons is of the same order as the number of harder gluons.

From Fig. 8 we observe that the spectrum of high momentum gluons achieves an exponential shape on a short time scale and almost as quick as the soft gluons. However, they have different slopes. At $t = 0.5$ fm/c the entire spectrum is to a good extent in agreement with a thermal fit taking $T \simeq 0.67$ GeV, which is indeed very close to the effective temperature of the system at this time [$T_{\text{eff}}(t = 0.5 \text{ fm/c}) = E/3N = 0.6$ GeV]. The transverse momentum spectrum achieves a thermal shape in hard and soft regions almost simultaneously. The presence of a thermal bath of soft gluons seems not to be a necessary condition

for the equilibration of hard gluons. Again, this is different from the picture invoked in the “Bottom-Up” scenario.

In [25] where the dynamics of SU(2) gauge fields in presence of an initial anisotropy in momentum space is studied, it is shown that the energy obtained from the particles by a Weibel-like plasma instability does not lead to an exponential buildup of transverse magnetic fields. Rather it is transferred into the ultraviolet modes via a rapid “avalanche”. This phenomenon, which was also discussed in [26], is similar to what we have observed during the very early thermalization of CGC (see Fig. 8). A more detailed study of such a highly nonlinear phenomenon is certainly needed.

For CGC initial condition with $\alpha_s = 0.1$ and $Q_s = 3$ GeV the rapid “avalanche” is again seen in from Fig. 9. The number of hard gluons with an exponential shape increases on

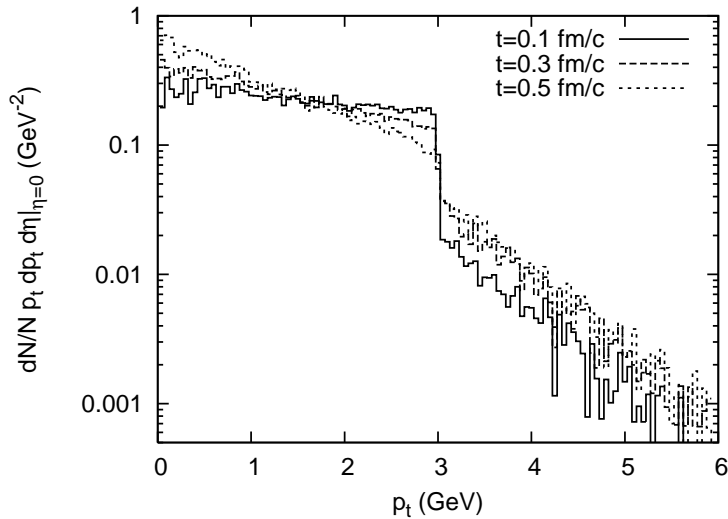


FIG. 9: Same as Fig.8. The initial condition is CGC with $\alpha_s = 0.1$ and $Q_s = 3$ GeV.

the same time scale as in the case for $\alpha_s = 0.3$. This can be understood from the following consideration: Because at early times I_{32} [see Eq. (9)] is roughly proportional to α_s^2 and the gluon density is inversely proportional to α_s , the initial interaction rate, $R_{32} \sim n^2 I_{32}$ [see Eq. (6)], is approximately independent of α_s .

Fig. 10 shows the transverse momentum spectra for $\alpha_s = 0.3$ at times larger than 0.5 fm/c. The spectra are compared with thermal fits using temperature T as a parameter. The effective temperatures $T = E/3N$, which is extracted from the simulations at various times, are found to be indeed close to the values chosen for the fits. Thus, the transverse spectrum

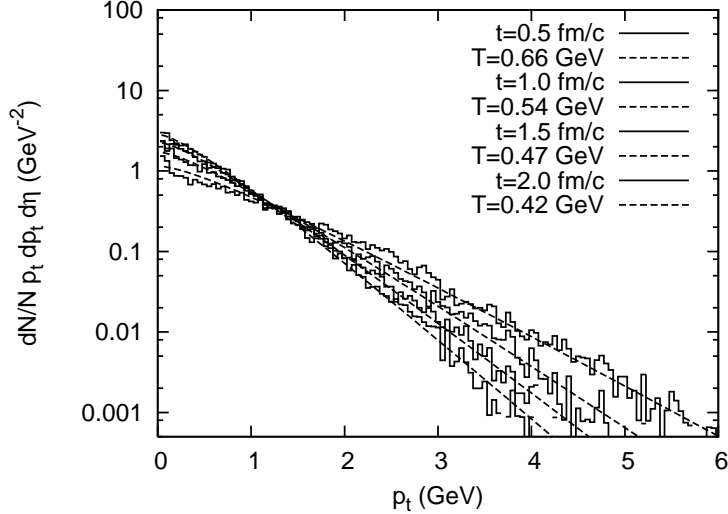


FIG. 10: Same as Fig.8 for later times.

at $t = 0.5$ fm/c looks almost thermal. Moreover, the cooling of the system sets in, which makes the exponential spectra steeper at later times. This behavior is characteristic for a hydrodynamical expansion.

Summarizing the results above, the thermalization of a CGC, studied in the parton cascade BAMPS, is characterized by the following facts to be opposed the “Bottom-Up” scenario:

- Emission of hard ($p_t > Q_s$) gluons due to $3 \rightarrow 2$ processes clearly dominates the very early evolution.
- No strong enhancement of total gluon number is observed. The total gluon number decreases slightly, until the system is nearly thermalized.
- No thermal bath of soft gluons is built up at very early times.
- Transverse momentum spectra achieves a thermal shape in the hard and soft regions almost simultaneously.

C. Time scale of thermalization

Next we extract the time scale when the system is more or less thermalized. A parametric dependence of the time scale, $\sim \alpha_s^{-13/5} Q_s^{-1}$, was given in the “Bottom-Up” scenario [7]. Fig.

11 shows the effective temperature, T , and the scaled one, $Tt^{1/3}$, as a function of time obtained with $\alpha_s = 0.3$ and $Q_s = 2, 3,$ and 4 GeV, respectively. The effective temperature

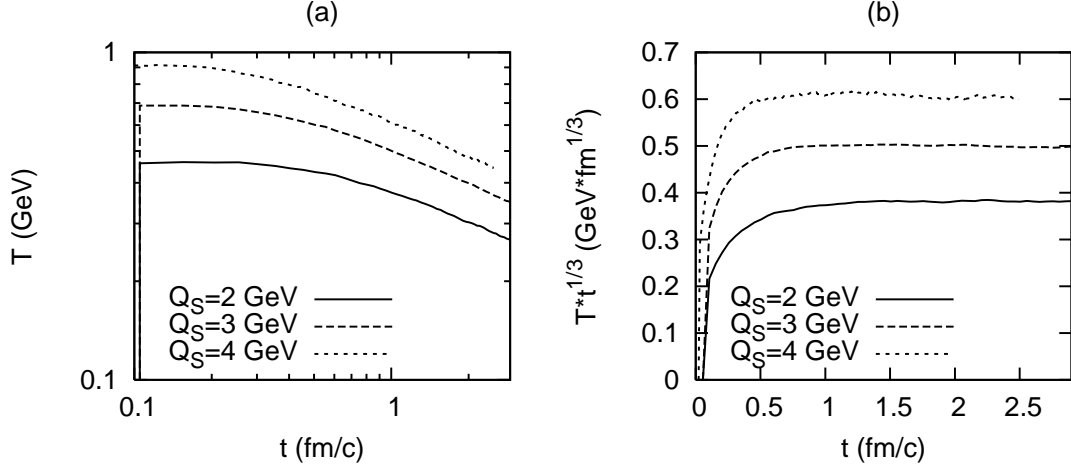


FIG. 11: (a) Effective temperature and (b) Scaled effective temperature.

increases slightly at very early times due to gluon annihilation and then falls approximately with $t^{-1/3}$ [see Fig. 11(b)]. The same scaling is also found for the transverse energy per rapidity at late times, as seen in Fig. 12(a), where $dE_T/dy \cdot t^{1/3}$ is depicted. The behavior

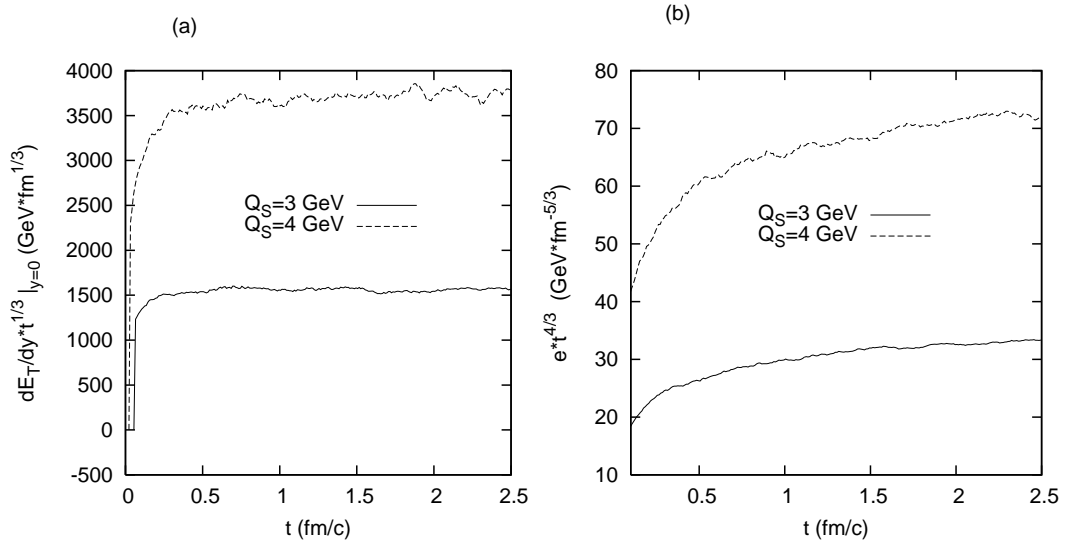


FIG. 12: (a) Scaled transverse energy per rapidity and (b) scaled energy density.

at late times corresponds to a one-dimensional ideal hydrodynamical expansion. Thus, we

determine the time scale of thermalization as the time, at which $Tt^{1/3}$ becomes a constant. The times extracted from Fig. 11(b) read:

$$t_{\text{th}}(Q_s = 2 \text{ GeV}) = 1.2 \text{ fm}/c, \quad t_{\text{th}}(Q_s = 3 \text{ GeV}) = 0.75 \text{ fm}/c, \quad t_{\text{th}}(Q_s = 4 \text{ GeV}) = 0.55 \text{ fm}/c. \quad (20)$$

The value for $Q_s = 3 \text{ GeV}$ is consistent with the time scale (0.5 fm/c) at which the transverse momentum spectrum becomes exponential (see Fig.10). In addition, the values of $t_{\text{th}} \cdot Q_s$ are almost equal for fixed α_s and various Q_s , which verifies the relation $t_{\text{th}} \sim Q_s^{-1}$ as predicted in the “Bottom-Up” scenario.

Although the expansion at late times is described nearly by ideal hydrodynamics, the collision rates are not infinitely high (see Fig. 5). Thus, the viscosity might be small but still nonzero (as shown in the next subsection). The effect of the nonzero viscosity is actually apparent in the scaled energy density, $e t^{4/3}$, depicted in Fig. 12(b). Although $e t^{4/3}$ is constant in time according to one-dimensional ideal hydrodynamics, $e t^{4/3}$ still increases at later times in the simulations.

For fixed $Q_s = 3 \text{ GeV}$ and various α_s the time scale of thermalization is extracted from Fig. 13 such that

$$t_{\text{th}}(\alpha_s = 0.1) = 1.75 \text{ fm}/c, \quad t_{\text{th}}(\alpha_s = 0.2) = 1 \text{ fm}/c, \quad t_{\text{th}}(\alpha_s = 0.3) = 0.75 \text{ fm}/c, \quad (21)$$

and

$$t_{\text{th}}\alpha_s^{13/5} = 0.0044 \text{ fm}/c(\alpha_s = 0.1), \quad 0.015 \text{ fm}/c(\alpha_s = 0.2), \quad 0.033 \text{ fm}/c(\alpha_s = 0.3). \quad (22)$$

The dependence of t_{th} on α_s proves to be considerable weaker in our cascade calculations compared to what is estimated in the “Bottom-Up” scenario. In Ref. [6] the authors found that the time scale of thermalization is the inverse of the total transport rate, which is proportional to $\alpha_s^{-2}(\ln \alpha_s)^{-2}T^{-1}$ [28] ($T \sim Q_s$ in the present case). This scaling indeed holds for the thermalization times from our calculations:

$$t_{\text{th}}\alpha_s^2(\ln \alpha_s)^2 = 0.09 \text{ fm}/c(\alpha_s = 0.1), \quad 0.1 \text{ fm}/c(\alpha_s = 0.2), \quad 0.1 \text{ fm}/c(\alpha_s = 0.3). \quad (23)$$

Therefore, the time scale of thermalization is of order $\alpha_s^{-2}(\ln \alpha_s)^{-2}Q_s^{-1}$, which is smaller than the “Bottom-Up” prediction. The quick thermalization observed here is consistent with the findings from the previous studies [5, 6, 13]: The gluon bremsstrahlung favors

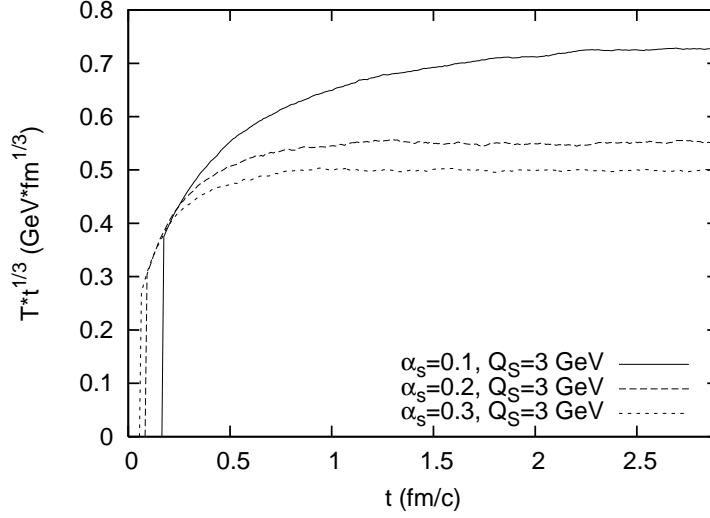


FIG. 13: Scaled effective temperature in simulations with fixed $Q_s = 3$ GeV and $\alpha_s = 0.1, 0.2,$ and 0.3 .

large-angle radiation due to the LPM suppression, which is the reason for the dominance of the pQCD $gg \leftrightarrow ggg$ processes in thermal equilibration.

Figure 14 shows the time evolution of the total gluon number per space time rapidity. The

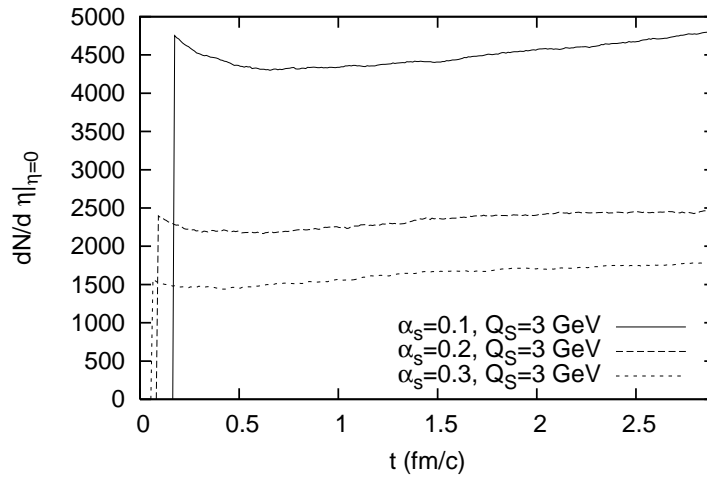


FIG. 14: Gluon number per space time rapidity in calculations with fixed $Q_s = 3$ GeV and $\alpha_s = 0.1, 0.2,$ and 0.3 .

initial condition with $\alpha_s = 0.2$ and $Q_s = 3$ GeV could be appropriate for Pb-Pb collisions

at the maximal energy at the LHC. In this case the gluon number also decreases at the beginning. Thus, “Bottom-Up” thermalization might not be favored at LHC.

Momentum isotropization, which is an important part of kinetic equilibration, can be described by the time evolution of $\langle p_z^2/E^2 \rangle$ [6] shown in Fig. 15, where CGC initial conditions are used with $\alpha_s = 0.3$ and $Q_s = 2, 3,$ and $4,$ respectively. $\langle \cdot \rangle$ denotes the average over gluons

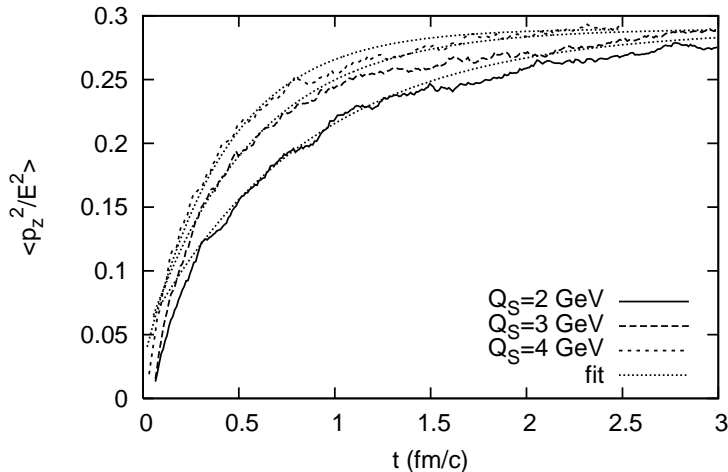


FIG. 15: Momentum isotropization. CGC initial conditions with $\alpha_s = 0.3$ and $Q_s = 2, 3,$ and $4,$ respectively.

in the central space time rapidity. Due to expansion, $\langle p_z^2/E^2 \rangle$, which is extracted in a finite spatial volume, saturates at a value that is slightly smaller than its equilibrium value $1/3$. We fit $\langle p_z^2/E^2 \rangle(t)$ at time t_0 using a relaxation ansatz

$$F(t) = \frac{1}{3} + \left(\left\langle \frac{p_z^2}{E^2} \right\rangle(t_0) - \frac{1}{3} \right) \exp \left(-\frac{t - t_0}{\theta_{\text{rel}}(t)} \right) \quad (24)$$

where θ_{rel} gives the time scale of momentum isotropization [6]. The fits are shown in Fig. 15. Using $t_0 = 0.5$ fm/c, we find $\theta_{\text{rel}} = 0.85, 0.52,$ and 0.42 fm/c for $Q_s = 2, 3,$ and 4 GeV, respectively. These time scales are smaller than thermalization time scales [see Eq.(20)], which indicates that momentum isotropization is completed before (nearly) full thermalization with quasi-ideal hydrodynamical expansion.

D. Ratio of the shear viscosity to the entropy density

As already noticed in the previous subsection, $e t^{4/3}$ increases slightly at later times [see Fig. 12(b)], which shows a deviation from ideal hydrodynamics. However, the agreements of $T t^{1/3}$ and $dE_T/dy \cdot t^{1/3}$ with ideal hydrodynamics [see Figs. 11 and 12(a)] indicates that the shear viscosity (or better the ratio of the shear viscosity to the entropy density) is small.

In the Navier-Stokes approximation, the diagonal elements of the stress tensor are given [27] in the rest frame by

$$T_{ii} = P - 2\eta \left(\frac{\partial u_i}{\partial x_i} - \frac{1}{3} \vec{\nabla} \cdot \vec{u} \right) - \kappa \vec{\nabla} \cdot \vec{u} \quad (25)$$

where η denotes the shear viscosity, κ the bulk viscosity, and P the pressure. We then obtain

$$\eta = \frac{T_{xx} + T_{yy} - 2T_{zz}}{2(3\partial_z u_z - \vec{\nabla} \cdot \vec{u})}, \quad (26)$$

$$\kappa = \frac{3P - T_{xx} - T_{yy} - T_{zz}}{3\vec{\nabla} \cdot \vec{u}}. \quad (27)$$

For the system of massless gluons where $e = 3P$, the bulk viscosity vanishes. The flow velocity \vec{u} is expected to be approximately the same as given in [14]. For an ideal hydrodynamical expansion $\vec{u} \approx (0, 0, z/t)$ when the gluonic system is (nearly) thermalized. Thus, we obtain

$$\eta = \frac{t}{4} (T_{xx} + T_{yy} - 2T_{zz}) \quad (28)$$

where T_{xx} , T_{yy} and T_{zz} can be extracted from the numerical calculations. Note that the divergence of the flow velocity can be better extracted from the simulations because it relates to the transport collision rate, as derived in [28].

Due to large numerical uncertainties the entropy density it is difficult to extract s from the simulations. Therefore, the formula

$$s = - \int \frac{d^3p}{(2\pi)^3} f_{\text{eq}}(p, x) [\ln f_{\text{eq}}(p, x) - 1] = 4n - n \ln(\lambda) \quad (29)$$

with $f_{\text{eq}}(p, x) = \lambda d_G e^{-\frac{E}{T}}$ is used, which is applied to systems in kinetic equilibrium. Here n is the gluon density and $\lambda = n/n_{\text{th}}$ denotes the gluon fugacity where $n_{\text{th}} = d_G T^3/\pi^2$ is the gluon density in thermal equilibrium. The entropy density calculated in Eq. (29) is, thus, larger than the true value in the simulations.

Figure 16 shows the η/s ratio in the calculations with $\alpha_s = 0.3$ and $Q_s = 2, 3,$ and 4 , respectively. Before $0.5 \text{ fm}/c$ the values of η/s are not reliable because at early times the

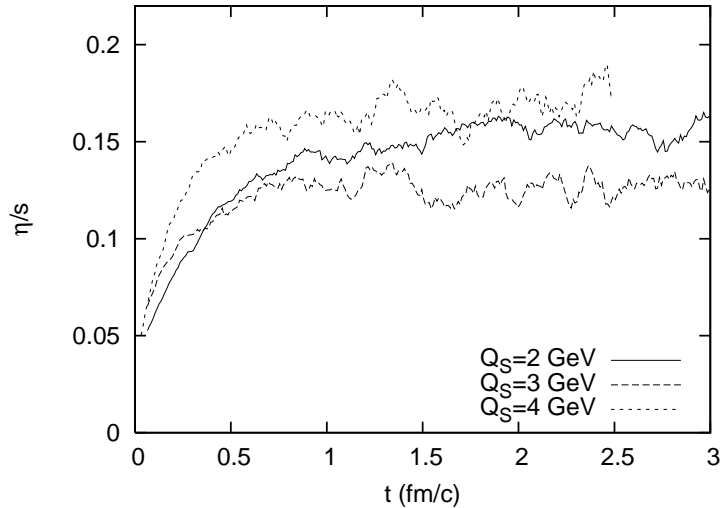


FIG. 16: Ratio of the shear viscosity to the entropy density. CGC initial conditions with $\alpha_s = 0.3$ and $Q_s = 2, 3,$ and $4,$ respectively.

gluon system is far from equilibrium and, thus, Eqs. (28) and (29) are not valid. From 0.5 fm/c on the η/s ratio is nearly constant and has a weak dependence on Q_s , $\eta/s \approx 0.15$, which is exactly the same as that obtained in full 3+1 dimensional BAMPS calculations with $\alpha_s = 0.3$ and minijets type initial conditions for Au+Au collisions at RHIC energies [29]. This verifies that the η/s ratio determines the behavior of the late dynamics and, thus, depends only on the coupling α_s , but not on initial conditions. Moreover, the η/s ratio obtained is small and close to the lower bound from the AdS/CFT conjecture [30]. The smallness of the η/s ratio corresponds to the efficiency of the pQCD $gg \leftrightarrow ggg$ processes in thermal equilibration, because the η/s ratio is inversely proportional to the total transport collision rate and the transport collision rate of $gg \leftrightarrow ggg$ processes is $6 - 7$ times larger than that of $gg \rightarrow gg$ collisions [28].

VI. CONCLUSION

Using the parton cascade BAMPS, we have studied the thermalization of potential color glass condensates, which might be appropriate for the initial conditions of high energy heavy ion collisions. The main emphasis is put on the comparison of the thermalization observed in our calculations to that in the “Bottom-Up” scenario. We found that several aspects

of the real thermalization might be different compared to the “Bottom-Up” scenario. The difference arises because the back reactions of bremsstrahlung, $3 \rightarrow 2$ processes, play a significant role. They are completely absent in the “Bottom-Up” scenario.

First, the radiation of gluons is hindered by $3 \rightarrow 2$ processes according to detailed balance. Therefore, for the idealistic form chosen for CGC, the total gluon number will increase unless $\alpha_s Q_s$ is very large, which is not realistic at RHIC and LHC. We showed that for realistic initial conditions the total gluon number decreases early in the expansion. An exorbitant increase in soft gluons, as predicted in the “Bottom-Up” scenario, is not possible. Thus, no thermal bath of soft gluons will be built up.

Second, thermal equilibration of soft and hard gluons occurs roughly on the same time scale due to $2 \rightarrow 3$ and $3 \rightarrow 2$ processes, respectively. The energy flows into both the soft and hard sectors at the same time, which is potentially similar to the phenomenon of “avalanche” as observed in the field isotropization driven by the plasma instability. This behavior contradicts the “Bottom-Up” picture where soft gluons form a thermal bath and thermalize first whereas hard gluons lose energy to the thermal bath and, thus, thermalize later.

Finally, the time scale of thermalization is determined for various values of α_s and Q_s . It spreads from 0.55 fm/c to 1.75 fm/c for $Q_s = 2 - 4$ GeV and $\alpha_s = 0.1 - 0.3$. In agreement with the “Bottom-Up” scenario, the thermalization time proves to be proportional to Q_s^{-1} , however, its proportionality to $\alpha_s^{-13/5}$ is not seen, but is much weaker: $\tau_{\text{th}} \sim (\alpha_s \ln \alpha_s)^{-2} Q_s^{-1}$.

After being thermalized the gluon system shows quasi-hydrodynamical behavior: The cooling due to expansion is observed in the steepening of the transverse momentum spectra. To see how viscous the system is, we extracted the ratio of the shear viscosity to the entropy density and obtained $\eta/s \approx 0.15$ for $\alpha_s = 0.3$. The η/s ratio has a weak dependence on Q_s and is close to the lower bound from the AdS/CFT conjecture. Thus, the considered gluon system acts as being strongly coupled.

The quick thermalization and the smallness of the η/s ratio observed in the present calculations with the CGC initial conditions are consistent with the findings from the previous studies [5, 6, 13, 28, 29] using the Glauber-type minijets initial conditions. This demonstrates that independent of the chosen initial conditions, the pQCD bremsstrahlung processes (and the back reactions) dominate the dynamical equilibration and then keep the system behaving like a nearly perfect fluid. The higher order processes such like $ggg \rightarrow ggg$

and $gg \leftrightarrow gggg$ will certainly lead to a larger total transition rate, however, their contributions are suppressed by higher order of α_s [31]. Further investigations are needed to quantify these contributions.

The CGC initial conditions presented in this paper are idealistic. More realistic initial conditions in high energy nucleus-nucleus collisions can be obtained by considering high momentum jet like partons(minijets)[32]. This will modify the thermalization picture presented in this paper: $ggg \rightarrow gg$ interaction may become less dominant at the early stage of the thermal equilibration, however, it would not affect our conclusion that thermalization in the hard and soft sectors proceeds on the same time scale. A study will be presented elsewhere.

Acknowledgments

A.E. gratefully acknowledges a fellowship by the Helmholtz foundation.

-
- [1] P. Huovinen, P. F. Kolb, U. W. Heinz, P. V. Ruuskanen, and S. A. Voloshin, Phys. Lett. B **503** (2001) 58 .
 - [2] S. S. Adler et al. [PHENIX Collaboration], Phys. Rev. Lett. **91** (2003) 182301 .
 - [3] J. Adams et al. [STAR Collaboration], Phys. Rev. Lett. **92** (2004) 052302 .
 - [4] S. Mrówczyński, Phys. Lett. B **314** (1993) 118 ; Phys. Rev. C **49** (1994) 2191; P. Arnold, J. Lenaghan, and G.D. Moore, J. High Energy Phys. **0308** (2003) 002; P. Arnold, J. Lenaghan, G.D. Moore, and L.G. Yaffe, Phys. Rev. Lett. **94** (2005) 072302; A. Rebhan, P. Romatschke, and M. Strickland, Phys. Rev. Lett. **94** (2005) 102303; A. Dumitru and Y. Nara, Phys. Lett. B **621** (2005) 89 .
 - [5] Z. Xu and C. Greiner, Phys. Rev. C **71** (2005) 064901.
 - [6] Z. Xu and C. Greiner, Phys. Rev. C **76** (2007) 024911.
 - [7] R. Baier, A. H. Mueller, D. Schiff, and D. T. Son, Phys. Lett. B **502** (2001) 5158.
 - [8] L. D. McLerran and R. Venugopalan, Phys. Rev. D **49** (1994) 2233; *ibid.* **49** (1994) 3352.
 - [9] A. Krasnitz and R. Venugopalan, Phys. Rev. Lett. **84** (2000) 4309 ; *ibid.* **86** (2001) 1717 .
 - [10] A. H. Mueller, Nucl. Phys. B **572** (2000) 227; Phys. Lett. B **475** (2000) 220.
 - [11] J. Bjorker and R. Venugopalan, Phys. Rev. C **63** (2001) 024609.

- [12] J. Serreau and D. Schiff, JHEP 0111 (2001) 039.
- [13] Z. Xu and C. Greiner, Eur. Phys. J. A **29** (2006) 33.
- [14] J. D. Bjorken, Phys. Rev. D **27** (1983) 140.
- [15] J. F. Gunion and G. Bertsch, Phys. Rev. D **25** (1982) 746.
- [16] T. S. Biro, E. van Doorn, B. Müller, M. H. Thoma, and X.-N. Wang, Phys. Rev. C **48** (1993) 1275.
- [17] S. M. H. Wong, Nucl. Phys. A **607** (1996) 442.
- [18] A. Krasnitz, Y. Nara, R. Venugopalan, Phys. Rev. Lett. **87** (2001) 192302 and Nucl. Phys. A **727** (2003) 427-436
- [19] T. Lappi, Phys. Rev. C **67** (2003) 054903
- [20] D. Khardeev, M. Nardi, Phys. Lett. B **507** (2001) 121
- [21] A. El, C. Greiner, Z. Xu, Nucl. Phys. A **785** (2007) 132c-137c
- [22] A. El, Diploma thesis at University Frankfurt am Main (2006)
- [23] C. Adler, et al., [STAR Collaboration], Phys. Rev. Lett. **87** (2001) 112303.
- [24] B. B. Back, et al., [PHOBOS Collaboration], Phys. Rev. C **70** (2004) 021902(R).
- [25] A. Dumitru, Y. Nara, and M. Strickland, Phys. Rev. D **75** (2007) 025016.
- [26] P. Arnold and G. D. Moore, Phys. Rev. D **73** (2006) 025006.
- [27] P. Danielewicz and M. Gyulassy, Phys. Rev. D **31** (1985) 53.
- [28] Z. Xu and C. Greiner, arXiv: 0710.5719 [nucl-th].
- [29] Z. Xu, C. Greiner, and H. Stöcker, arXiv: 0711.0961 [nucl-th].
- [30] G. Policastro, D. T. Son and A. O. Starinets, Phys. Rev. Lett. **87** (2001) 081601; P. K. Kovtun, D. T. Son and A. O. Starinets, Phys. Rev. Lett. **94** (2005) 111601.
- [31] L. Xiong, E.V. Shuryak, Phys. Rev. C **49** (1994) 2203.
- [32] A. Adil, H.-J. Drescher, A. Dumitru, A. Hayashigaki, Y. Nara, Phys. Rev. C **74** (2006) 044905.